Inorganic Chemistry

Article

pubs.acs.org/IC

Reactivity of Coordinatively Unsaturated Bis(N-heterocyclic carbene) Pt(II) Complexes toward H_2. Crystal Structure of a 14-Electron Pt(II) Hydride Complex

Orestes Rivada-Wheelaghan,[†] Marta Roselló-Merino,[†] Manuel A. Ortuño,[‡] Pietro Vidossich,[‡] Enrique Gutiérrez-Puebla,[§] Agustí Lledós,*[,‡] and Salvador Conejero*[,†]

[†]Departamento de Química Inorgánica, CSIC and Universidad de Sevilla, Instituto de Investigaciones Químicas (IIQ), Avda. Américo Vespucio 49, 41092, Sevilla, Spain

[‡]Departament de Química, Universitat Autònoma de Barcelona, 08193, Cerdanyola del Vallès, Spain

[§]Instituto de Ciencia de Materiales de Madrid, ICMM-CSIC, Cantoblanco, 28049, Madrid, Spain

Supporting Information

ABSTRACT: The reactivity toward H_2 of coordinatively unsaturated Pt(II) complexes, stabilized by N-heterocyclic carbene (NHC) ligands, is herein analyzed. The cationic platinum complexes $[Pt(NHC')(NHC)]^+$ (where NHC′ stands for a cyclometalated NHC ligand) react very fast with H_2 at room temperature, leading to hydrogenolysis of the Pt−CH_2 bond and concomitant formation of hydride derivatives $[PtH(NHC)_2]^+$ or hydrido−dihydrogen complexes $[PtH(H_2)(NHC)_2]^+$. The latter species release H_2 when these compounds are subjected to vacuum. The X-ray structure of complex $[PtH(IPr)_2][SbF_6]$ revealed its unsaturated nature, exhibiting a true T-shaped structure without stabilization by agostic interactions. Density functional theory calculations indicate that the binding and reaction of H_2 in complexes $[PtH(H_2)(NHC)_2]^+$ is more favored for derivatives bearing aryl-substituted NHCs (IPr, 1,3-bis(2,6-diisopropylphenyl)-imidazol-2-ylidene and IMes = 1,3-dimesityl-1,3-dihydro-2H-imidazol-2-ylidene) than for those containing *tert*-butyl groups (I^tBu). This outcome is related to the higher close-range steric effects of the I^tBu ligands. Accordingly, H/D exchange reactions between hydrides $[PtH(NHC)_2]^+$ and D_2 take place considerably faster for IPr and IMes* derivatives than for I^tBu ones. The reaction mechanisms for both H_2 addition and H/D exchange processes depend on the nature of the NHC ligand, operating through oxidative addition transition states in the case of IPr and IMes* or by a σ-complex assisted-metathesis mechanism in the case of I^tBu.

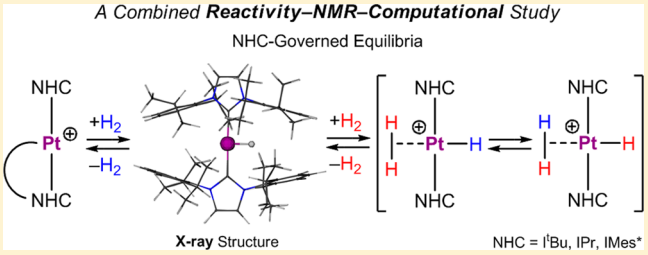

INTRODUCTION

The catalytic dehydrogenation of amine−boranes, and particularly ammonia−borane, has emerged as a powerful method for the generation of dihydrogen under mild conditions.[1] Several transition-metal complexes are known to be active in this process.[1d,2] Recently, we have reported that the low-electron count Pt(II) complex $[Pt(I^tBu')(I^tBu)][BAr^F]$ **1a** (where I^tBu is 1,3-di-*tert*-butyl-imidazol-2-ylidene and I^tBu' is the cyclometalated ligand) is able to dehydrogenate dimethylamine−borane (DMAB) very efficiently at room temperature.[3] We have seen that at the end of the reaction the released dihydrogen hydrogenates the Pt−CH_2 bond of the catalyst, leading to platinum hydride $[PtH(I^tBu)_2][BAr^F]$ as the sole platinum reaction product. This result contrasts with the partial hydrogenation of Pt−CH_2 bonds of electron-deficient cyclometalated Pt(II) species based on phosphine ligands.[4,5] Therefore, it is of paramount importance to analyze the reactivity of dihydrogen[6] toward coordinatively unsaturated Pt(II) complexes[7] and the affinity of H_2 to bind this metal center. In fact, in spite of the large number of dihydrogen complexes known at present,[8] very few are based on platinum, and in all cases phosphines have been used as ancillary ligands.[9] In this sense, although N-heterocyclic carbenes (NHCs) have been extensively used as an alternative to traditional phosphine ligands in transition-metal complexes, their ability to stabilize dihydrogen species has been scarcely explored.[10] The first organometallic compounds containing both dihydrogen and NHC ligands in the same coordination sphere, $(IMes)_xRu(H)_2(\eta^2\text{-}H_2)_2(PCy_3)_{2-x}$ (IMes = 1,3-dimesityl-1,3-dihydro-2*H*-imidazol-2-ylidene; x = 1, 2), were reported in 2003.[11] The influence of the size of the N substituent on the NHC ligand on the interaction with H_2 has been demonstrated by the study of the reactivity with H_2 of the three five-coordinate ruthenium NHC hydrido complexes $[Ru(I^iPr_2Me_2)_4H]^+$ ($I^iPr_2Me_2$ = 1,3-diisopropyl-4,5-dimethylimidazol-2-ylidene), $[Ru(IEt_2Me_2)_4H]^+$ (IEt_2Me_2 = 1,3-diethyl-4,5-dimethylimidazol-2-ylidene), and $[Ru(IMe_4)_4H]^+$ (IMe_4 = 1,3,4,5-tetramethylimi-

Received: March 26, 2014
Published: April 9, 2014

   dx.doi.org/10.1021/ic500705t | *Inorg. Chem.* 2014, 53, 4257−4268

dazol-2-ylidene).[12] Variation of the N substituents provides some control on the H_2 binding: $[Ru(I^iPr_2Me_2)_4H]^+$ is unreactive, $[Ru(IEt_2Me_2)_4H]^+$ coordinates H_2 only at low temperature and incompletely, while $[Ru(IMe_4)_4H]^+$ affords the dihydrogen complex in quantitative yield at room temperature. Density functional theory (DFT) calculations supported the experimental findings, showing that $[Ru(IMe_4)_4H]^+$ exhibits the strongest computed binding energy for H_2.

Herein, we report the reactivity of some 14-electron Pt(II) alkyl complexes stabilized by NHC ligands[13] toward H_2, leading to 14-electron Pt(II) hydride species and, in some cases, to Pt(II) hydrido−dihydrogen derivatives. The experimental work is complemented by computational studies that tackle both structural and reactivity aspects of the system.

RESULTS AND DISCUSSION

Reactivity Studies of Complexes $[Pt(NHC')(NHC)]^+$ (1a−d) toward H_2. In previous papers[13] we have reported the synthesis of 14-electron Pt(II) complexes bearing some of the NHC ligands shown in Figure 1 (I^tBu **a**, IPr **b**, and IMes* **c**) (IPr = 1,3-bis(2,6-diisopropylphenyl)imidazol-2-ylidene). In this work the ligand $I^iPr_2Me_2$ **d** was also considered. From now onward, the notation NHC′ stands for the cyclometalated ligand.

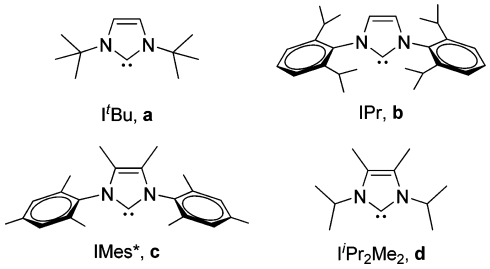

Figure 1. N-Heterocyclic carbene ligands used in this and previous works.[13]

When a solution of complex $[Pt(I^tBu')(I^tBu)][BAr^F]$ **1a** was pressurized under a dihydrogen atmosphere in a J. Young NMR tube in CD_2Cl_2, a rapid color change from yellow to colorless was observed at room temperature. The ^1H NMR spectrum at this temperature revealed the formation of a new hydride species $[PtH(I^tBu)_2][BAr^F]$, **2a**, resulting from the addition of a dihydrogen molecule across the Pt−CH_2 bond (Scheme 1).[14]

Scheme 1. Hydrogenation of Complex 1a

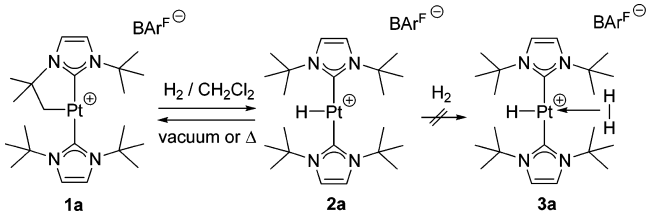

Both carbene ligands are now equivalent, and only two signals are discernible in the ^1H NMR spectrum for the protons of the *tert*-butyl groups and the backbone of the imidazolyl ring. The hydride signal resonates as a sharp singlet at −25.55 ppm with a very large coupling constant to ^{195}Pt of 2564 Hz, comparable to that reported for the phosphine analogue $[PtH(P^tBu_3)_2]^+$ (ca. 2570 Hz).[15] No indication of dihydrogen coordination (forming putative species **3a**) is evident from the ^1H NMR experiment, even at low temperature (−80 °C), nor is there evidence of the presence of agostic interactions. Unfortunately, in spite of the stability of **2a** under dihydrogen atmosphere, it transforms very rapidly into the cyclometalated species **1a** under vacuum or by slight heating in dichloromethane.

The complete hydrogenation of the starting material contrasts with the partial hydrogenation of their phosphine counterparts $[Pt(PR_3')(PR_3)]^+$ (where PR_3' denotes the cyclometalated phosphine ligand).[4] These complexes partially react with H_2 giving rise to equilibrium mixtures of the Pt(II) hydrido complexes $[PtH(PR_3)_2]^+$ and the starting material. This equilibrium is shifted to the hydride complex when more basic phosphines are used. Therefore, the better electron-donor properties of NHCs[16] compared to phosphines might be responsible for the exclusive observation of platinum hydride **2a** in solution.

We have also examined the reactivity of the cyclometalated complex $[Pt(IPr')(IPr)][BAr^F]$ **1b** toward H_2 (Scheme 2).[17]

Scheme 2. Hydrogenation of Complex 1b

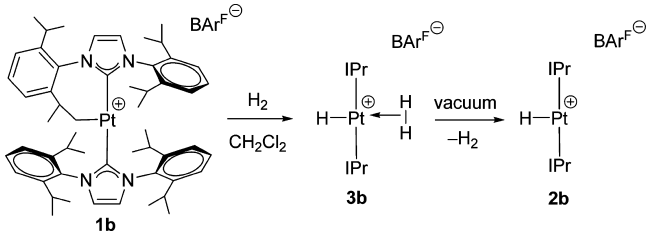

When this complex is reacted with dihydrogen in a J. Young NMR tube under identical conditions as for complex **1a**, a new compound is formed with a very symmetrical environment. According to its ^1H NMR spectrum, only one set of signals appeared for the IPr ligands. However, at variance with complex $[PtH(I^tBu)_2]^+$ **2a**, no hydride signals were observable at room temperature in the hydride region of the ^1H NMR spectrum. The absence of resonances due to Pt−H signals led us to consider that if a hydride were present at the Pt center, it might be involved in a fluxional process. To slow down such a process, the ^1H NMR experiment was recorded at −40 °C. At this temperature two signals with doublet (−0.78 ppm) and triplet (−12.28 ppm) multiplicities were clearly discernible, integrating for two and one protons, respectively, including satellites due to couplings to ^{195}Pt. These signals appeared in the same region as the hydrido−dihydrogen derivatives $[PtH(\eta^2\text{-}H_2)(PR_3)_2][BAr^F]$ (R = ^{t}Bu, ^{i}Pr, Cy)[9c−e] with similar $^1J_{H,H}$ and $^1J_{H,Pt}$ coupling constants, leading us to postulate the presence of the dihydrogen species $[PtH(\eta^2\text{-}H_2)(IPr)_2][BAr^F]$ **3b** (Scheme 2). Short T_1 values (and $^1J_{H,D}$ couplings as described below) support the formulation of a Pt(II) hydrido−dihydrogen complex. Although a minimum value could not be confirmed, qualitative T_1 values were obtained at −50 °C. At this temperature the coordinated H_2 resonance has a T_1 value of 27 ms (400 MHz), consistent with a dihydrogen bound ligand. The hydride signal at −12.28 ppm has a long T_1 value of 1.056 s, suggesting that, on the NMR time scale, no H/H_2 exchange is occurring.

Compound **3b** is perfectly stable in solution under dihydrogen atmosphere, but releases a molecule of H_2 very easily under vacuum to yield the platinum hydride derivative

dx.doi.org/10.1021/ic500705t | Inorg. Chem. 2014, 53, 4257−4268

$[PtH(IPr)_2][BAr^F]$ **2b** (Scheme 2). At variance with compound $[PtH(I^tBu)_2][BAr^F]$ **2a**, the IPr derivative **2b** does not undergo cyclometalation to revert to **1b** either under vacuum or at room temperature. This reaction only takes place when complex **2b** is subjected to mild heating in dichloromethane. The stability of complex **2b** in the solid state allowed us to fully characterize this species by spectroscopic and X-ray methods. Crystals of complex **2b**·SbF_6 suitable for X-ray diffraction studies were obtained by slow diffusion of concentrated solutions of **2b**·SbF_6 in dichloromethane into pentane. As can be seen in Figure 2, the structure consists of two IPr ligands in a trans arrangement (C12_i–Pt–C12 angle = 178.5(1)°) and a hydride ligand (located in the Fourier map). No other ligand was found trans to the hydride, in spite of crystallizing the complex in dichloromethane solution at low temperature.[9d] The SbF_6 anion is too far from the metal center to consider any possible interaction. The Pt1–C12 and Pt1–C12_i bond distances are 2.029(3) Å, and the Pt1–H101 separation has a value of 1.67(2) Å. The dihedral angle of 35.2(4)° formed by the N1–C12–C12_i–N1_i atoms compares well with related derivatives. The most notable feature of this structure is the true vacant site trans to the hydride ligand, where no agostic interactions are present. The closest H and C atoms of methyl groups of the isopropyl fragments are located at 2.53(5) and 3.471(5) Å, respectively, which are considerably longer than the expected distances for agostic interactions.[18] The DFT-optimized geometry is in good agreement with the experimental structure (Figure 2).

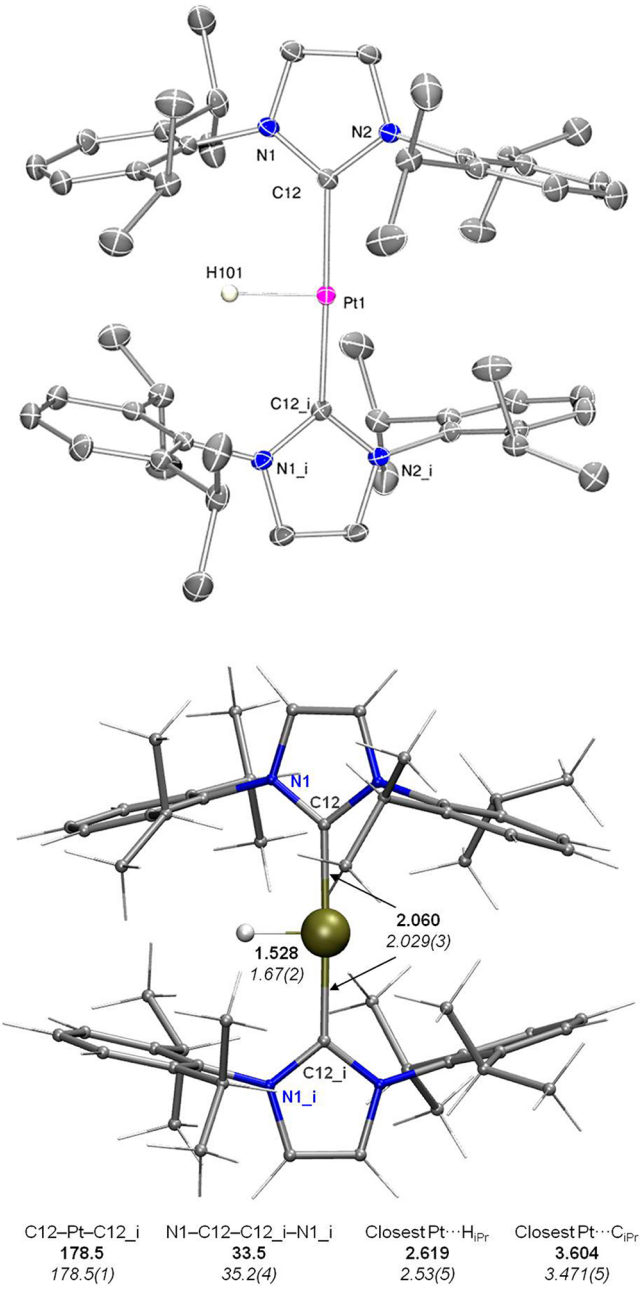

Figure 2. (top) ORTEP representation of the cation of complex **2b**·SbF_6. Thermal ellipsoids are drawn at 50% probability level. SbF_6 anion and hydrogen atoms, except the hydride ligand, were omitted for clarity. (bottom) Theoretical (bold) and experimental (italic) parameters of **2b**. Bond distances in Å and angles in degrees.

The lack of agostic interactions in complex **2b** might be related to structural features such as ligand flexibility.[19] On the other hand, the high trans influence of the hydride ligand might also play a role.[20] Similar effects have been reported by Braunschweig and co-workers in Pt(II) complexes bearing very high trans influence boryl ligands.[21] However, agostic interactions in a trans position to hydride ligands have been observed in a related Ir(III) complex bearing I^tBu NHCs.[14] Coordinatively unsaturated transition-metal complexes bearing the very small hydride ligand that have been characterized by X-ray diffraction methods are extremely rare,[22] and this is the first fully structurally characterized example of a true 14-electron Pt(II) hydrido complex.

The ^1H NMR spectrum of derivative **2b** exhibits a broad signal in the hydride region at −35.86 ppm with a very large coupling constant to ^{195}Pt of 2669 Hz, the largest ever reported to the best of our knowledge. Low-temperature NMR experiments were performed to find evidence of agostic interactions in CD_2Cl_2 solutions. Nevertheless, no signs of such interactions were seen. Instead, two species were detected in the ^1H NMR spectrum at −50 °C in ca. 3:2 ratio, with no agostic interactions being observed for either of the two complexes. Both compounds exhibit signals in the hydride region at −28.50 ppm ($^1J_{H,Pt}$ = 1902 Hz) and −34.19 ppm ($^1J_{H,Pt}$ = 2712 Hz), respectively. The large coupling constant to ^{195}Pt observed for the latter suggests that this corresponds to the 14-electron Pt(II) complex $[PtH(IPr)_2][BAr^F]$ **2b**. However, the relatively small $^1J_{H,Pt}$ value (1902 Hz) recorded for the other hydride signal points to the presence of a ligand located in its trans position. In fact, the lower the temperature, the higher the proportion of this species. Considering that the ^1H NMR signals of the IPr ligands for this new species are still highly symmetric, it is very unlikely that this effect is due to the presence of an agostic interaction, which would produce a larger $^1J_{H,Pt}$ value for the Pt–H moiety (ca. 2090 Hz).[4b] Instead, it is reasonable that coordination of a dichloromethane solvent molecule to form the adduct $[PtH(ClCD_2Cl)(IPr)_2][BAr^F]$ **2b**·CD_2Cl_2 is occurring at this temperature. Kubas and co-workers reported that dichloromethane can indeed form adducts with the Pt(II) hydride $[PtH(P^iPr_3)_2][BAr^F]$, for which the hydride signal resonates at −22.82 ppm with a similar coupling to ^{195}Pt ($^1J_{H,Pt}$ = 1852 Hz).[9d,23]

With regard to the infrared (IR) spectrum of complex **2b**, no distinguishable Pt–H band is observed. The Pt–H stretching frequency is probably masked by those of the C–H stretching vibrations of the IPr ligands (2800–2900 cm^{-1}), as previously observed for the Pt(II) complex $[PtH(P^tBu)_3)_2]^+$.[15]

dx.doi.org/10.1021/ic500705t | Inorg. Chem. 2014, 53, 4257–4268

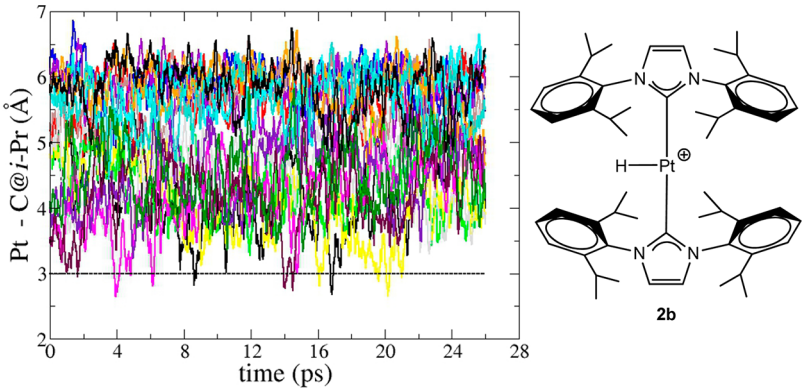

Figure 3. Distances from Pt to the methyl C atoms of the ^{i}Pr groups of the IPr ligands during the QM/MM MD simulation of **2b**. The dashed black line indicates the Pt···C distance of the stable agostic interaction observed in **1b**.[19]

To shed light on the conformational fluctuations of **2b** in solution, molecular dynamics (MD) simulations were carried out using a quantum mechanics/molecular mechanics (QM/MM) description of the system. Dichloromethane (DCM) solvent was considered explicitly, treating the complex at DFT level[24] and the solvent at MM level (about 1000 DCM molecules, see Computational Details). Twenty-six picosecond simulations were performed for the **2b** and **2b**·CH_2Cl_2 species. We were interested in looking at (i) whether agostic interactions are formed and (ii) the possibility of formation of **2b**·CH_2Cl_2 adducts. The simulation was started from the X-ray structure of **2b**, where no agostic interaction is present between Pt and the substituents of the IPr ligands. Accordingly, no agostic interactions are formed during the simulation. Figure 3 clearly shows that all Pt···C$_{^{i}Pr}$ distances display values larger than 3.5 Å along the entire simulation. Although the methyl C atoms from the ^{i}Pr groups may occasionally attend short distances to the Pt center, a stable interaction never takes place. This finding is in contrast with the behavior of the corresponding cyclometalated compound **1b**, which was shown to display an agostic interaction in solution characterized by a Pt···C distance of ca. 3 Å.[19]

To investigate the formation of the adduct **2b**·CH_2Cl_2, we promoted a DCM molecule to the QM system to properly describe the binding situation and steered it toward the Pt center. This procedure was repeated twice, using different initial conditions and steering different DCM molecules, and produced similar results. A stable **2b**·CH_2Cl_2 indeed forms via a Pt···Cl interaction. Figure 4 shows that the interaction is maintained throughout the span of the simulation (8 ps). From these results we may rule out the formation of agostic species, and attribute the signals observed in the low temperature ^{1}H NMR spectrum to **2b** and **2b**·CH_2Cl_2.

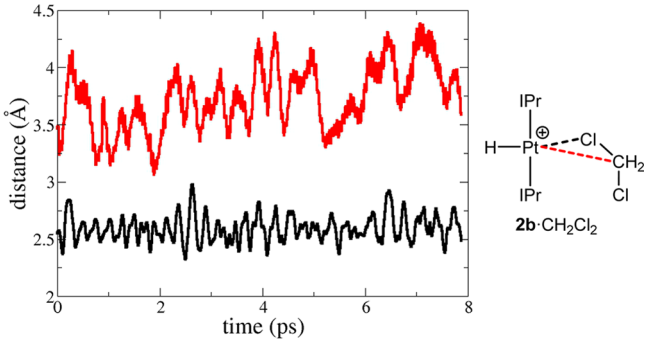

Figure 4. Distances from Pt to Cl (black line) and C (red line) atoms of the coordinating dichloromethane molecule during the QM/MM MD simulations of **2b**·CH_2Cl_2.

Complex **1c** also reacts very fast with H_2 in dichloromethane (Scheme 3). The resulting complex shows some similarities to the hydrogenation products of complexes **1a** and **1b**. The room temperature ^{1}H NMR spectrum of the crude reaction mixture formed upon exposing derivative **1c** to H_2 (2 bar) in a J. Young NMR tube resulted in the clean formation of a complex that contains two equivalent IMes* ligands and a rather broad hydride signal resonating at −22.54 ppm with a $^{1}J_{H,Pt}$ of ca. 2110 Hz. Curiously, in spite of the large excess of dihydrogen present in solution, no signal for free H_2 was detected, contrary to the result found in the hydrogenation of complex **1a**. Therefore, a fluxional process involving dihydrogen might be occurring at this temperature. However, the observation of the hydride signal in the ^{1}H NMR spectrum, even at this temperature, contrasts with its absence in complex [PtH(H_2)-(IPr)$_2$]$^{+}$ **3b** at room temperature, but very much resembles that of complex [PtH($I^{t}Bu$)$_2$]$^{+}$ **2a**. Consequently, low-temperature NMR experiments were carried out to explain this different behavior. At −50 °C, the ^{1}H NMR spectrum (under a 2 bar H_2 atmosphere) indicates the presence of three different species in a ratio of ca. 9:9:2. On the basis of their ^{1}H NMR data, the two major species were identified as the platinum hydride [PtH(IMes*)$_2$][BAr^{F}] **2c** and the dihydrogen complex [PtH-(η^2-H_2)(IMes*)$_2$][BAr^{F}] **3c**, whereas the minor one was tentatively identified as the dichloromethane adduct **2c**·

Scheme 3. Hydrogenation of Complex 1c

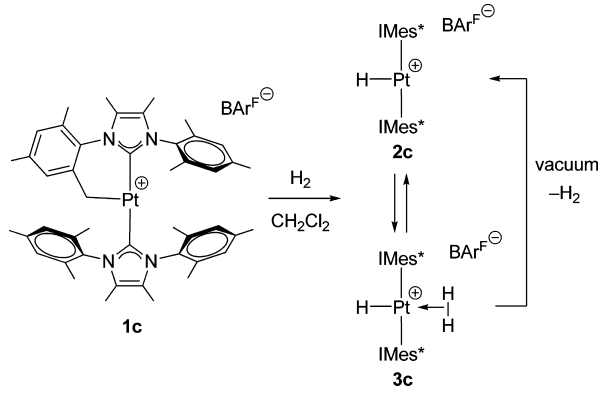

dx.doi.org/10.1021/ic500705t | Inorg. Chem. 2014, 53, 4257−4268

CD_2Cl_2. Complex **3c** shows signals for the hydride and dihydrogen ligands with chemical shifts and coupling constants to ^{195}Pt similar to derivative **3b** (Pt−H: −12.91 ppm, $^1J_{H,Pt}$ = 1912 Hz; Pt−H_2: −0.94 ppm, $^1J_{H,Pt}$ = 187 Hz). The hydride signal of derivative **2c** appears at −24.35 ppm ($^1J_{H,Pt}$ = 2228 Hz), while that for the dichloromethane adduct **2c**·CD_2Cl_2 resonates at −28.80 ppm, with a coupling to ^{195}Pt ($^1J_{H,Pt}$ = 1994 Hz) similar to **2b**·CD_2Cl_2.[25] Therefore, the three species **2c**, **3c**, and **2c**·CD_2Cl_2 coexist in equilibrium at this temperature. Note that contrary to IPr derivative **b**, the most shielded species is the adduct **2c**·CD_2Cl_2. As expected, an increase of the dihydrogen pressure in the NMR tube to 5 bar results in an increase of the dihydrogen complex present in solution at −50 °C (11:2.5:2 ratio for **3c**/**2c**/**2c**·CD_2Cl_2).

As was observed for **2b**, QM/MM MD simulations for **2c** in dichloromethane solvent reveal that stable agostic interactions do not take place in this system. From the simulations the average distance from Pt to C atoms of the ortho methyl groups on IMes* ranges from 4.0 to 4.3 Å (see Supporting Information), ruling out Pt···HC interactions. These parameters indicate that the methyl substituents of the phenyl rings on IMes* cannot approach the Pt center closely enough to form stable agostic interactions.

Complex **3c** is unstable under vacuum conditions, releasing a molecule of H_2 with concomitant formation of the Pt(II) hydride derivative **2c**. This latter compound is perfectly stable under argon and does not undergo cyclometalation at room temperature. The ^1H NMR spectrum of **2c** recorded at −50 °C indicates the presence of two compounds, the coordinatively unsaturated **2c** and its dichloromethane adduct **2c**·CD_2Cl_2.

Finally, the hydrogenation of complex **1d**, bearing $I^iPr_2Me_2$ ligands **d**, was attempted to analyze the effect of a less bulky ligand on the stability of the final products. Unfortunately, when derivative **1d** was reacted with H_2 in dichloromethane at room temperature several products of unknown composition were formed. Nonetheless, the hydrogenation of the Pt−CH_2 bond, leading to the complex [PtH(THF)($I^iPr_2Me_2$)$_2$][BAr^F], **2d**·THF, does occur in tetrahydrofuran (THF) solvent. The reaction is very slow at room temperature (12 h) but can be accelerated at 55 °C, taking place in 2.5 h. This different reactivity with respect to complexes **1a**−**c** is probably related to the formation of a very stable adduct of complex **1d** with THF, which prevents, to some extent, the hydrogenation reaction.[26] In the ^1H NMR spectrum the hydride signal of compound **2d**·THF resonates at −28.09 ppm with a $^1J_{H,Pt}$ of 1930 Hz, which is considerably lower than that observed for the analogous hydride complexes **2a**−**c**. This coupling constant is halfway between the values observed for complexes **2a**−**c** and the THF adducts *trans*-[PtH(THF)(PR_3)$_2$]$^+$ (R = ^{i}Pr, Ph),[9d,27] suggesting that reversible coordination of THF might be occurring in complex **2d**·THF. In fact, compound **2d**·THF decomposes in dichloromethane solutions into the same products observed during hydrogenation of **1d** in dichloromethane. Therefore, decomposition pathways not available for its bulkier counterparts **2a**−**c** may be feasible for a putative **2d** species due to the reduced steric bulk of the $I^iPr_2Me_2$ ligands.

Reactivity Studies of Complexes [PtH(NHC)$_2$]$^+$ (2a−c) toward D_2. It was shown that the dihydrogen complexes **3b** and **3c** seem to be fluxional (Schemes 2 and 3). With a view to further investigate the nature of this process, we carried out some reactions between the Pt(II) hydride complexes **2a**−**c** and D_2.

When solutions of complexes **2b** or **2c** were exposed to 1 bar of D_2 at room temperature (Scheme 4), a rather fast H/D

Scheme 4. Deuteration of Complexes 2a−c

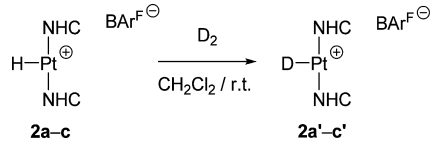

scrambling of the hydride signals was observed by NMR spectroscopy (less than 45 min for completion). Under these conditions, no deuteration of the methyl groups of IPr **b** or IMes* **c** ligands was observed. Therefore, only the hydride ligand in complexes **2b** and **2c** is exchanging with D_2. In these reactions, the residual η^2-DH complexes [PtD(η^2-DH)(NHC)$_2$][BAr^F] permitted observation of a H−D coupling constant of 35 Hz, in good agreement with the estimated T_1 values and the formulation of a dihydrogen complex.[8e,28]

The H/D exchange entails the rupture of the D−D bond and the formation of a H−D bond. Several mechanisms can be devised for such a process,[29] which will be analyzed in the Computational Section (see below).

On the other hand, complex **2a** also undergoes H/D scrambling with D_2, but the process is remarkably slow, taking ca. 5 d to reach 70% of deuterium incorporation, under otherwise identical conditions to those for complexes **2b** and **2c**. Kubas and co-workers reported that H/D scrambling was not observed in the related Pt(II) hydride species [PtH(P^iPr_3)$_2$]$^+$, but caution should be taken since this experiment was run over a period of only 20 min.[9d] The underlying reasons for this different behavior in our systems are not entirely clear but are obviously related to the lower propensity of complex **2a** to coordinate a molecule of H_2. This point will be investigated with DFT calculations (see below).

Computational Study of the Reactivity of Complexes [Pt(NHC′)(NHC)]$^+$ (1a−c) toward H_2. To rationalize the different behavior of the cyclometalated compounds [Pt(NHC′)(NHC)]$^+$ (**1a**−**c**) toward the addition of H_2, we have explored these reactions at the DFT level using the M06 functional, which accounts for dispersion interactions[30] (see Computational Details). The process initiates by H_2 coordination to the empty position of the cyclometalated species (intermediates **1-H$_2$**). At this point, several routes can lead to the hydride species **2** (Scheme 5). In presence of excess of H_2, dihydrogen can coordinate the vacant position of **2**, leading to the dihydrogen complexes **3a**-**c**. Regarding the H_2 addition step, it can entail a sequential oxidative addition/reductive elimination (OA/RE) process through a transient Pt(IV) dihydride species **1**−**2H**. This process can also take place in a concerted manner through a so-called oxidative addition transition state (OATS via **TS1**−**2**). A direct hydrogen transfer from the η^2-H_2 ligand to the methylene group of the cyclometalated NHC ligand, with no change on the oxidation state of platinum, can also occur. This mechanism has been termed σ-complex assisted metathesis (σ-CAM),[29c] although several situations may exist, depending on the degree of interaction of the metal with the hydrogen being transferred in the transition state.[29b] In this latter mechanism the ligands exchanging the hydrogen atom (η^2-H_2 and CH_2 of NHC′) must occupy mutually cis positions. Thus, a trans−cis

dx.doi.org/10.1021/ic500705t | Inorg. Chem. 2014, 53, 4257−4268

Scheme 5. Hydrogenation Reaction Mechanisms under Consideration

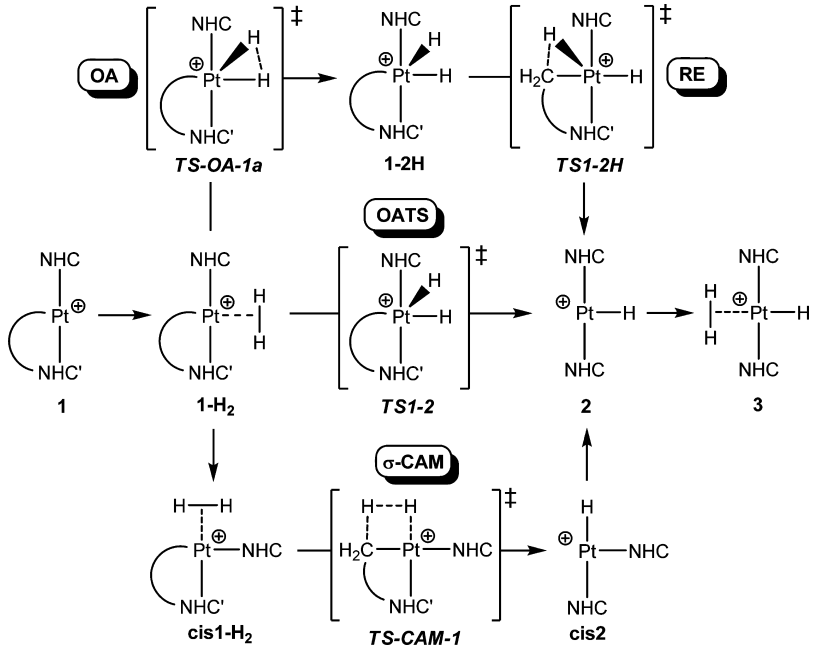

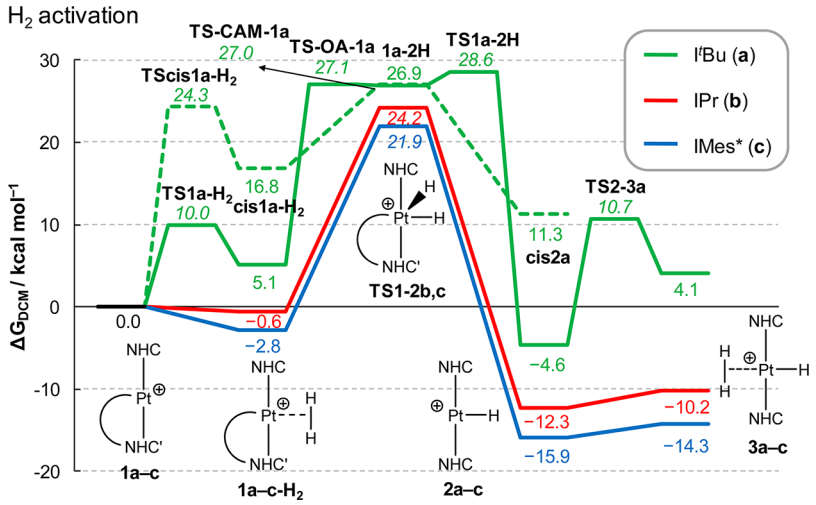

Figure 5. Gibbs energy profiles in dichloromethane (kcal mol^{-1}) for the reaction of **1a–c** with H_2. Complexes **1a–c** + 2 H_2 were taken as zero of energies.

isomerization of the NHC ligand should happen in **1** prior to the H–H bond breaking.

Gibbs energy profiles in dichloromethane, summarizing the hydrogenation of **1a–c**, are depicted in Figure 5. The relative energies of the intermediates and transition states in both mechanisms exhibit notable differences, depending on the nature of the NHC ligands. Looking at the OA/RE mechanism, the Pt(IV) dihydrido species is found as a very shallow minimum for the hydrogenation of **1a**, but it exhibits a transition-state nature for **1b** and **1c**. Subsequent hydrogenolysis of the Pt–CH_2 bond gives the Pt(II) hydrido complexes **2a–c**. The reaction of **1a** with H_2 displays the highest Gibbs energy profile (Figure 5, solid green line). The H–H bond breaking takes place in a two-step mechanism involving oxidative addition and reductive elimination processes through a five-coordinate Pt(IV) dihydrido intermediate **1a-2H**. The overall reaction of **1a** demands 28.6 kcal mol^{-1} via **TS1a-2H**,[31] and the resulting hydrido complex **2a** is 4.6 kcal mol^{-1} more stable than **1a**. It is worth noting that the mainly entropic barrier to H_2 coordination in **1a** and **2a** is not compensated by the Pt–H_2 interaction, giving rise to a barrier when H_2 approaches **1a** (**TS1a-H$_2$**, 10.0 kcal mol^{-1} above **1a**) and **2a** (**TS2–3a**, 15.3 kcal mol^{-1} above **2a**). Indeed, coordination of a dihydrogen molecule to **2a** forming **3a** is not favored, the latter lying 8.7 kcal mol^{-1} above **2a**.

The Gibbs energy profiles for the H_2 addition to **1b** and **1c** along the OATS pathway are very similar (Figure 5, red and blue lines, respectively). Contrary to species with ligands **a**, the corresponding barriers of H_2 coordination to **1b** and **1c** forming **1b-H$_2$** and **1c-H$_2$**, respectively, were not found when ligands **b** and **c** are involved. The subsequent hydrogenolysis via **TS1–2b** and **TS1–2c** requires overcoming almost the same barrier for **1b-H$_2$** as for **1c-H$_2$** (24.8 and 24.7 kcal mol^{-1}, respectively). The resulting hydrido products **2b** and **2c** are much more stable than **2a**, preventing their transformation back to the cyclometalated species. As for **1b** and **1c**, H_2

dx.doi.org/10.1021/ic500705t | Inorg. Chem. 2014, 53, 4257–4268

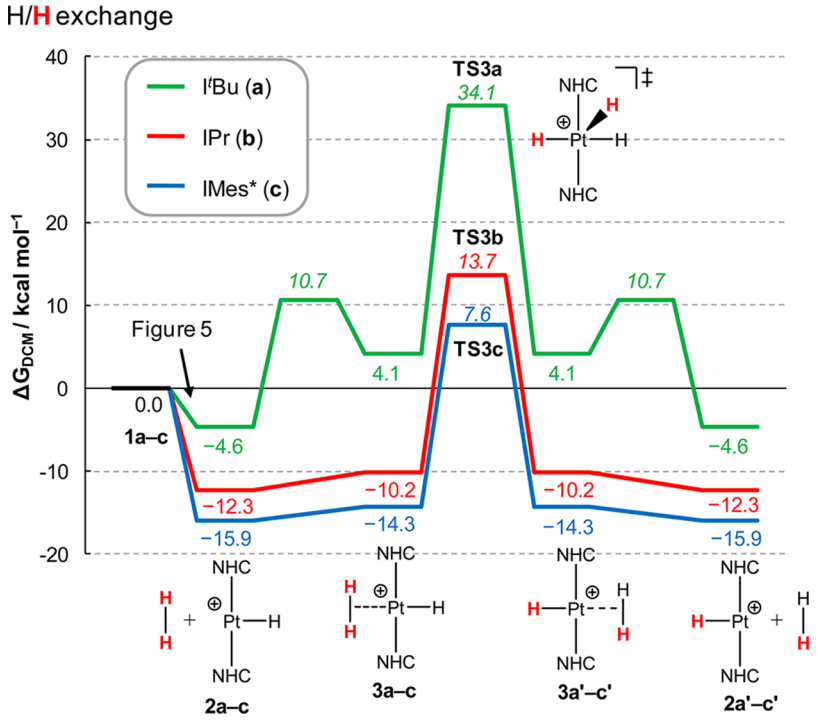

Figure 6. Gibbs energy profiles in dichloromethane (kcal mol^{-1}) for the hydrogen exchange in **2a**–**c** through an OATS mechanism. Complexes **1a**–**c** + 2 H_2 were taken as zero of energies.

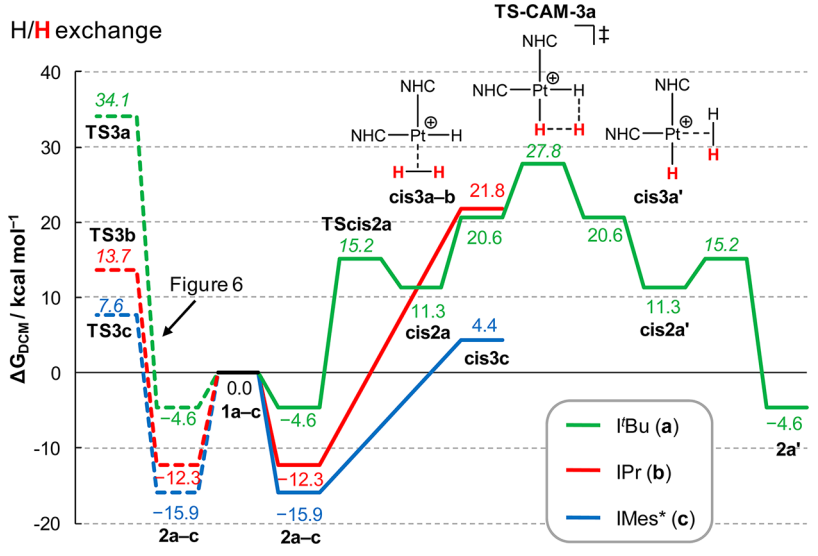

Figure 7. Gibbs energy profiles in dichloromethane (kcal mol^{-1}) for the hydrogen exchange in **2a**–**c** through a σ-CAM mechanism. Complexes **1a**–**c** + 2 H_2 were taken as zero of energies.

coordination to **2b** and **2c** proceeds with no activation barrier, giving rise to the adducts **3b** and **3c** that are only slightly above **2b** and **2c**. The similar relative Gibbs energies of **2b**/**2c** and **3b**/**3c** ($\Delta\Delta G_{DCM}$ of 2.1 and 1.6 kcal mol^{-1} for ligands **b** and **c**, respectively) agree with the observed equilibria. The main differences arise in the relative stabilities of the addition products **2b**, **2c**, **3b**, and **3c** with respect to **1b** and **1c**. The more electron-donating IMes* stabilizes more efficiently than IPr both the hydrido (**2c**) and hydrido–dihydrogen (**3c**) complexes.[16]

Concerning the σ-CAM mechanism (Scheme 5), the Gibbs energy profile in dichloromethane for the H_2 addition to **1a** is also shown in Figure 5 (dashed green line). The concomitant approaching of H_2 and displacement of the NHC ligand toward the vacant position in **1a** forms the intermediate **cis1a-H$_2$**, which contains the η^2-H_2 ligand cis to the methylene group of the NHC′ ligand. It is 11.7 kcal mol^{-1} less stable than the trans isomer (**1a-H$_2$**), and it is reached after crossing a barrier of 24.3 kcal mol^{-1} (**TScis1a-H$_2$**). Then the σ-CAM process, via **TS-CAM-1a**, entails a barrier of 27.0 kcal mol^{-1} and produces the hydrido complex **cis2a** placed at 11.3 kcal mol^{-1} above **1a**. Intermediate **cis2a** connects to **2a** through **TScis2a** (see below, Figure 7). Overall, **TS-CAM-1a** demands 27.0 kcal mol^{-1},[31] which is 1.6 kcal mol^{-1} less than **TS1a-2H**; thus, the σ-CAM route is slightly favored over the OA/RE for **1a**. From **2a**, the

dx.doi.org/10.1021/ic500705t | Inorg. Chem. 2014, 53, 4257–4268

reaction could revert to the initial products with a barrier of 31.6 kcal mol^{-1}.

Given that the transition state involved in the trans−cis isomerization for **1a** has already the same energy as the transition states for the OA/RE pathway in **1b** and **1c**, higher trans−cis isomerization barriers are expected for the latter species. As a result, we have not followed the σ-CAM mechanism for the complexes **1b** and **1c** bearing bulkier NHC ligands.

To sum up, the highest Gibbs energy barrier for the H_2 addition concerns the reaction of complex **1a** and demands 27.0 kcal mol^{-1}, whereas the process requires ca. 25 kcal mol^{-1} for **1b** and **1c**. Larger differences are found in the stability of the H_2 addition products. In the case of ligand **a**, **2a** is not much more stable than **1a** (4.6 kcal mol^{-1}), but it is much more stable than **3a** (8.7 kcal mol^{-1}), precluding its detection. On the contrary, **2b** and **2c** are much more stable than the parent **1b** and **1c** complexes. In addition, **2b,c** and **3b,c** have similar energies, in agreement with the equilibria experimentally observed.

Structural comparison between compounds **2** and **3** provides a rationale for the role played by the NHC ligand on the stability of the H_2 adducts **3.** Table 1 reports the N−C−C−N dihedral angle between the two NHC ligands in **2** and **3**, namely, ϕ. On one hand, a considerable rearrangement of the I^{t}Bu ligands is required to form **3a**; that is, the NHCs evolve from perpendicular to an almost coplanar orientation. On the other hand, small variations are found for IPr (**b**) and IMes* (**c**) ligands. A distortion energy analysis[13a,32] was carried out to estimate the energy penalty for such a NHC reorientation (Table 1). The H_2 ligand was removed from **3**, obtaining the distorted species **3^d**. The gas-phase energy difference between **2** and **3^d**, namely ΔE_{dist}, accounts for the energy required to create the empty space that H_2 will fill in **3**. The higher distortion energy of **3^{d}a** (9.1 kcal mol^{-1}) with respect to **3^{d}b** and **3^{d}c** (ca. 3−4 kcal mol^{-1}) suggests that steric factors are playing a role.[33] Although IPr and IMes* are still bulky ligands, no large rearrangement is required to coordinate the small H_2 molecule. ΔE_{dist} values correlate fairly with the relative stabilities between **2** and **3** (Table 1).

Table 1. Selected Dihedral Angles, Distortion Energies in Gas-Phase, and Gibbs Energies in DCM

NHC	ϕ(2), deg	ϕ(3), deg	ΔE_{dist} (**2**→**3^d**)^a	ΔG_{DCM}(**3** − **2**)^a
I^{t}Bu **a**	87.0	16.1	9.1	8.7
IPr **b**	48.1	40.7	3.3	2.1
IMes* **c**	35.5	33.1	3.8	1.6

^{a}Energy in kcal mol^{-1}

These results might be related to the different steric effects of NHC ligands, usually discussed in terms of percent of volume buried $\%V_{bur}$.[34,35] *Tert*-butyl groups in I^{t}Bu exert an important steric hindrance in the nearby proximity to the metal center, whereas aryl substituents in IPr and IMes* lay further from the platinum atom. In this regard, it should be pointed out that according to $\%V_{bur}$ values, the bulkiness of IPr and I^{t}Bu ligands is quite similar. However, this model is based on the "*percent of a total volume of a sphere occupied by a ligand*".[35] Commonly the radius of this sphere is set at 3.5 Å from the metal, but when set at 3.0 Å, the $\%V_{bur}$ of I^{t}Bu is larger than that of IPr, which translates into a more congested environment in the immediacy of the metal center.[34b] Indeed, for a small ligand such as H_2, close-range effects prevail. In agreement with this, Table 2 shows the computed $\%V_{bur}$ at different radius values for several NHCs extracted from the structures of **2a−c**. I^{t}Bu (**a**) remains almost the same, whereas IPr (**b**) and IMes* (**c**) become less bulky at short radii, that is, in the proximity of the metal.

Table 2. Computed Volume Buried Values ($\%V_{bur}$) of a−c Ligands at Different Radii

	$\%V_{bur}$			
NHC	R = 2.5 Å	R = 3.0 Å	R = 3.5 Å	R = 4.0 Å
I^{t}Bu **a**	39.1	39.9	38.9	37.1
IPr **b**	34.0	38.0	41.4	43.7
IMes* **c**	30.4	34.1	36.8	38.4

Computational Study of the Hydrido−Dihydrogen Exchange of Complexes [PtH(NHC)$_2$]$^+$ (2a−c). We have theoretically analyzed the hydrido−dihydrogen exchange[36] that accounts for the H/D scrambling observed in the presence of D_2 for **2a−c** (Scheme 4). Coordination and ulterior addition of D_2 to **2a−c** produce the deuterides **2a′−c′** and a HD molecule. As for the H_2 addition described above, we considered two possible mechanisms for this reaction (Scheme 6): an oxidative addition transition state (OATS) process through Pt(IV) trihydrido species (Figure 6) and a σ-CAM mechanism,[29c] in which the hydrogen exchange takes place via intermediates with the two NHC ligands mutually cis (Figure 7).

First, the OATS reaction mechanism was computed for complexes **2a−c** (Figure 6). Calculations indicate that for the hydride complexes with IPr (**2b**) and IMes* (**2c**) ligands, the hydrogen exchange via OATS is feasible (Figure 6, red and blue lines, respectively). The Pt(IV) trihydrido transition states **TS3b** and **TS3c** are placed 26.0 and 23.5 kcal mol^{-1} above **2b** and **2c**, respectively. For **2b** the barrier for the H/D exchange (26.0 kcal mol^{-1}) is slightly higher than that for the H_2 addition to **1b** (24.8 kcal mol^{-1}), suggesting that the exchange is slower than the H_2 addition. However, complex **2c** follows the opposite trend; in this case the H/D exchange (23.5 kcal mol^{-1}) becomes faster than the H_2 addition to **1c** (24.7 kcal mol^{-1}). On the other hand, the H/D exchange of **2a** requires 38.7 kcal mol^{-1} via **TS3a**, which makes such OATS process not feasible for complexes with I^{t}Bu ligands (Figure 6, green line).

As an alternative, the σ-CAM mechanism was also considered (Figure 7). The first step of this pathway requires a cis disposition of the NHC ligands. With the more bulky IPr **b** and IMes* **c** ligands (Figure 7, red and blue lines, respectively), the cis hydrido−dihydrogen intermediates are placed above (**cis3b** at 21.8 kcal mol^{-1}) or close (**cis3c** at 4.4 kcal mol^{-1}) to the corresponding OATS transition states (**TS3b** at 13.7 and **TS3c** at 7.6 kcal mol^{-1}, respectively). For **2b** the σ-CAM pathway can be clearly discarded. For **2c**, although the intermediate **cis3c** is 3.2 kcal mol^{-1} more stable than **TS3c**, the putative σ-CAM transition state is likely higher in energy. Thus, this reaction mechanism can also be ruled out. This is not the case for I^{t}Bu ligand **a** (Figure 7, green line), in which the σ-CAM mechanism entails a barrier considerably lower (**TS-CAM-3a**, 32.4 kcal mol^{-1} above **2a**) than that of the OATS pathway (**TS3a**, 38.7 kcal mol^{-1} above **2a**). In any case, the barrier for the exchange of the hydride ligand with H_2 in **2a** is substantially higher than it is in **2b** and **2c**. As a conclusion, the H/D exchange proceeds through an OATS mechanism for **2b** and **2c** but involves a σ-CAM process for **2a**. The latter complex **2a** demands higher Gibbs energy barriers than those for **2b** and **2c**, in agreement

dx.doi.org/10.1021/ic500705t | Inorg. Chem. 2014, 53, 4257−4268

Scheme 6. Hydrogen Exchange Mechanisms under Consideration

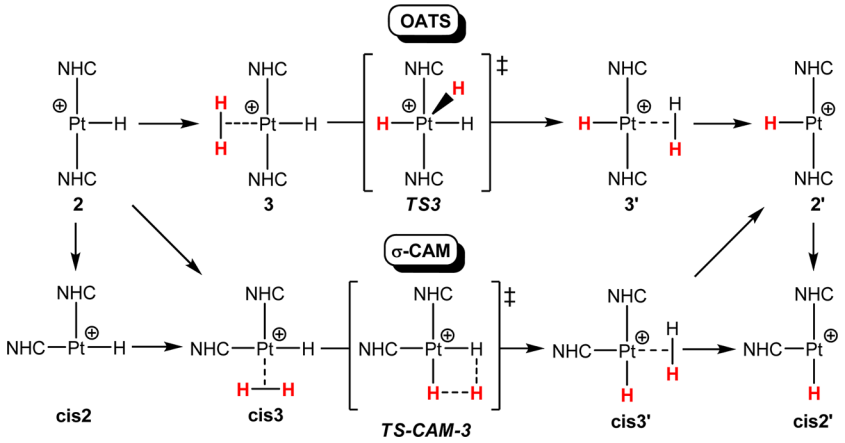

with the much slower H/D scrambling experimentally observed.

CONCLUSIONS

The reactivity of the cyclometalated compounds [Pt(NHC′)(NHC)][BAr^F] with H_2 leads to the formation of either coordinatively unsaturated Pt(II) hydride species [PtH(NHC)$_2$][BAr^F] or dihydrogen complexes [PtH(η^2-H_2)(NHC)$_2$][BAr^F], depending on the nature of the NHC. The ligand $I^iPr_2Me_2$ is not sufficiently bulky to stabilize the corresponding Pt(II) hydrido complexes [PtH($I^iPr_2Me_2$)$_2$][BAr^F], decomposing in weak-coordinating solvents, such as dichloromethane. We have crystallographically characterized the first coordinatively unsaturated Pt(II) hydride complex [PtH(IPr)$_2$][SbF_6], which is not stabilized by agostic interactions. Platinum hydride complexes [PtH(NHC)$_2$][BAr^F] undergo H/D scrambling at considerably different rates when exposed to D_2, being much faster for the NHC ligands IPr and IMes*.

DFT calculations are in agreement with experimental observations regarding the better stabilization of dihydrogen complexes by IPr and IMes* ligands than by I^tBu. Computational studies on both the hydrogenolysis reaction of the Pt–CH_2 bond and the H/D exchange suggest that oxidative addition processes are more likely to occur for complexes bearing IPr and IMes* ligands, whereas a σ-CAM mechanism is favored when I^tBu ligands are involved. As experimentally observed, the Gibbs energy barriers involving complexes with I^tBu are higher than those concerning species with IPr and IMes*. Consequently, the nature of the NHC ligand determines the ability of their complexes to bind and activate H_2. Electronic effects are unlikely to be responsible of this effect since the σ electron-donor properties of the NHCs follow the trend IMes* > I^tBu > IPr.[16d] We believe that the proximity of the *tert*-butyl groups of the I^tBu ligand to the metal center destabilizes the formation of the σ-H_2 complex **3a**. This effect must be considered when developing catalytic systems for hydrogen production.

EXPERIMENTAL SECTION

General Comments. Manipulation of air- and moisture-sensitive compounds was performed under argon atmosphere using standard Schlenk techniques, employing dry solvents and glassware. High-resolution fast atom bombardment (FAB) mass spectra were recorded on an AutoSpec-Q mass spectrometer at the Instrumental Services of the Universidad de Sevilla (CITIUS). IR spectra were recorded on a PerkinElmer system 2000 FT-IR (nujol or KBr). NMR spectra were recorded on DRX-500, DRX-400, and DPX-300 spectrometers. Spectra were referenced to external $SiMe_4$ (δ = 0 ppm), using the residual protio-solvent peaks (^{1}H NMR experiments) or the characteristic resonances of the solvent nuclei (^{13}C NMR experiments) as internal standard. Spectral assignments were made by routine one- and two-dimensional NMR experiments (COSY, HSQC, HMBC, NOESY) where appropriate. The complexes [Pt(I^tBu')(I^tBu)][BAr^F] **1a**, [Pt(IPr′)(IPr)][X] (X = BAr^F, SbF_6) **1b**, and [Pt(IMes*′)(IMes*)][BAr^F] **1c** were prepared according to known methods.[13]

Synthesis of [PtH(I^tBu)$_2$][BAr^F], 2a. Complex [Pt(I^tBu')(I^tBu)][BAr^F], **1a** (50 mg), was dissolved in 0.7 mL of CD_2Cl_2 in a J. Young NMR tube with a screw cap. The solution was frozen, the headspace was evacuated, and H_2 was introduced at 2 bar. The initially yellow solution became colorless in about 5 min. The ^{1}H NMR spectrum, recorded at room temperature, indicated full conversion to complex **2a**. This compound is unstable under vacuum, releasing a molecule of H_2 and regenerating compound **1a**. ^{1}H NMR (500 MHz, CD_2Cl_2, 25 °C) δ: 7.18 (s, 4 H), 1.79 (s, 36 H; 12 Me-I^tBu), −25.55 (s + d, 1H, $^1J_{H,Pt}$ = 2564 Hz, Pt–H). ^{13}C{^{1}H} NMR (125 MHz, CD_2Cl_2, 25 °C) δ: 169.3 ($C_{carbene}$-Pt, $^1J_{Pt,C}$ = 1070 Hz, I^tBu), 118.2 (s, $^3J_{C,Pt}$ = 33 Hz, =CH), 59.0 (C_q-$(CH_3)_3$), 30.8 (s, 12 CH_3).

Synthesis of [PtH(η^2-H_2)(IPr)$_2$][BAr^F], 3b, [PtH(η^2-H_2)(IMes*)$_2$][BAr^F], 3c, [PtH(IPr)$_2$][BAr^F], 2b, and [PtH(IMes*)$_2$][BAr^F], 2c. Complex *trans*-[Pt(IPr′)(IPr)][SbF_6], **1b**·SbF_6 (0.04 mmol) (or **1b** [Pt(IPr′)(IPr)][BAr^F], 0.0.27 mmol or [Pt(IMes*′)(IMes*)][BAr^F], **1c** (0.03 mmol)) (50 mg) was dissolved in 0.7 mL of CD_2Cl_2 in a J. Young NMR tube with a screw cap. The solution was frozen, the headspace was evacuated, and H_2 was introduced at 2 bar. The initially yellow solution became immediately pale yellow. The ^{1}H NMR spectrum, recorded at room temperature, indicated full conversion to complexes **3b** and **3c** that are only stable in the presence of a positive pressure of H_2. Evaporation to dryness led to complexes **2b** and **2c**, which can be crystallized as yellow crystals by slow diffusion of solutions of **2b** and **2c** in CH_2Cl_2 into a diethyl ether/pentane mixture (3:10, **2b**) or pentane (**2c**) (83% yield for **2b** and 92% for **2b**·SbF_6; 75% yield for **2c**). **3b**: ^{1}H NMR (400 MHz, CD_2Cl_2, −40 °C) δ: 7.45 (t, 4H; Ph–H_p), 7.12 (d, 8H; Ph–H_m), 7.10 (s, 4H; =CH), 2.15 (sept, 8H, $^3J_{H,H}$ = 7 Hz; C***H***$(CH_3)_2$), 0.99 and 0.83(d, 24H each; $^3J_{H,H}$ = 7 Hz; CH(C***H***$_3)_2$), −0.78 (d + dd, 2H, $^3J_{H,H}$ = 23 Hz, $^2J_{H,Pt}$ = 224 Hz,Pt–(H_2)), −12.28 (t + dt, 1H, $^3J_{H,H}$ = 23 Hz, $^2J_{H,Pt}$ = 1818 Hz, Pt–H). ^{13}C{^{1}H} NMR (101 MHz, CD_2Cl_2, −40 °C) δ: 170.5 (Pt–$C_{carbene}$, $^1J_{Pt,C}$ = 1072 Hz), 144.9 (Ph–C_o), 136.1 (C_q-N), 131.0 (Ph–CH_p), 124.9 (Ph–CH_m), 124.6 (=CH), 28.9 (***C***H$(CH_3)_2$), 24.8, 23.9 (CH(***C***$H_3)_2$). **2b**: ^{1}H NMR (400 MHz, CD_2Cl_2, 25 °C) δ: 7.49 (t, 4H; Ph-H_p), 7.17 (d, 8H; Ph-H_m), 6.97 (s, 4H; =CH), 2.34 (sept, 8H, $^3J_{H,H}$ = 7 Hz; C***H***$(CH_3)_2$), 1.05 and 0.85(d, 24H each; $^3J_{H,H}$ = 7 Hz; CH(C***H***$_3)_2$), −35.86 (br s + d, 1H, $^1J_{H,Pt}$ = 2669 Hz, Pt–H). ^{13}C{^{1}H} NMR (100 MHz, CD_2Cl_2, 25 °C °C) δ: 179.3 (Pt–$C_{carbene}$, $^1J_{Pt,C}$ = 1154 Hz), 145.6 (Ph–C_o), 134.7 (C_q-N), 131.1 (Ph–CH_p), 124.9

dx.doi.org/10.1021/ic500705t | Inorg. Chem. 2014, 53, 4257−4268

(Ph−CH_m), 124.8 (=CH), 29.0 ($CH(CH_3)_2$), 24.6, 23.9 ($CH(CH_3)_2$). High-resolution mass spectrometry (HRMS) (FAB) *m/z:* calcd for $C_{54}H_{73}N_4Pt$: 972.5483. Found: 972.5504. **2c**: ^{1}H NMR (400 MHz, CD_2Cl_2, 25 °C) δ: 7.76 (s, 8H; Ph_{BArF}-CH_o), 7.59 (s, 8H; Ph_{BArF}−CH_m), 6.98 (s, 8H; Ph−CH_m), 2.43 (s, 12H; *p*-CH_3), 1.77 (s, 12H; =CCH_3), 1.71 (s, 24H; *o*-CH_3), −25.40 (s+d, 1H, $^1J_{H,Pt}$ = 2183 Hz, Pt−H). $^{13}C\{^1H\}$ NMR (101 MHz, CD_2Cl_2, 25 °C): 171.0 (Pt−$C_{carbene}$, $^1J_{Pt,C}$ = 1080 Hz), 162.1 (q, $^1J_{B,C}$ = 50 Hz, C_{ipso}-B), 139.0 (C_q, Ph−C_p), 135.3 (C_q, Ph−C_o), 135.1 (C_0, BAr^F), 133.7 (C_q−N), 129.2 (Ph−CH_m), 129.1 (q, $^2J_{C,F}$ = 30 Hz, C_m−BAr^F), 125.9 (=CCH_3), 124.5 (q, $^2J_{C,F}$ = 274 Hz, CF_3), 117.8 (C_p−BAr^F), 20.8 (*p*-CH_3), 17.3 (O−CH_3), 8.7 (=CCH_3). HRMS (FAB) *m/z:* calcd for $C_{46}H_{57}N_4Pt$: 860.4231. Found: 860.4200. **3c**: ^{1}H NMR (400 MHz, CD_2Cl_2, −50 °C) 7.76 (s, 8H; Ph_{BArF}−CH_o), 7.59 (s, 8H; Ph_{BArF}−CH_m), 6.85 (s, 8H; Ph−CH_m), 2.36 (s, 12H; *p*-CH_3), 1.73 (s, 12H; =CCH_3), 1.55 (s, 24H; *o*-CH_3), −0.94 (d + dd, 2H, $^1J_{H,H}$ = 20 Hz, $^1J_{H,Pt}$ = 187 Hz, Pt−(H_2))),)), −12.91 (t + dt, 1H, $^3J_{H,H}$ = 20 Hz, $^2J_{H,Pt}$ = 1912 Hz, Pt−H) .

Synthesis of Complex [PtH($I^iPr_2Me_2$)$_2$(d_8-THF)][BAr^F], 2d·d_8-THF. This species is prepared in situ from a solution of [Pt($I^iPr_2Me_2$′)($I^iPr_2Me_2$)][BAr^F] in d_8-THF that is charged with 1 atm of H_2 in a J. Young tube and stirred overnight at room temperature. Species **2d**·d_8-THF is stable in d_8-THF after the sample is degassed and the H_2 atmosphere is replaced with argon, but decomposes in CD_2Cl_2 at room temperature to some unidentified platinum hydrides. ^{1}H NMR (400 MHz, d_8-THF, 25 °C) δ 7.79 (m, 8H, Ph_{BArF}−CH_o), 7.58 (m, 4H, Ph_{BArF}−CH_m), 5.72 (br, 4H, C***H***$(CH_3)_2$), 2,24 (s, 12H, =CC***H***$_3$), 1.62 (d, $^3J_{HH}$ = 6.80 Hz, 24H, CH(C***H***$_3$)$_2$), −28.09 (s + d, $^1J_{PtH}$ = 1930 Hz, 1H, Pt−H). $^{13}C\{^1H\}$ NMR (101 MHz, d_8-THF, 25 °C) δ 172.7 (Pt−$C_{carbene}$), 163.0 (q, $^1J_{B,C}$ = 50 Hz, C_{ipso}−B), 135.8 (C_0, BAr^F), 130.2 (q, $^2J_{C,F}$ = 30 Hz, C_m−BAr^F), 126.1 (=***C***CH_3), 125.7 (q, $^2J_{C,F}$ = 274 Hz, CF_3), 118.4 (C_p−BAr^F), 53.9 (***C***$H(CH_3)_2$), 22.2 (CH(***C***$H_3)_2$), 10.2 (=C***C***H_3). The low stability of this compound precluded obtaining it in pure form.

H/D Exchange Reactions. Complexes 2b and 2c. Complex *trans*-[PtH(IPr)$_2$][SbF_6], **2b**·SbF_6 (0.025 mmol), or [PtH(IMes*)$_2$]-[BAr^F], **2c** (0.017 mmol), (30 mg) was dissolved in 0.7 mL of CD_2Cl_2 in a J. Young NMR tube with a screw cap. The solution was frozen, the headspace was evacuated, and D_2 was introduced at 1 bar at room temperature. The ^{1}H NMR recorded after 45 min indicated that H/D exchange occurred almost quantitatively, with only about 5% of the starting material remaining unreacted. Complex **2a**: Complex **2a** is first generated in situ in a J. Young NMR tube as described before. Excess H_2 is then removed by applying two freeze−pump−thaw cycles. Subsequently 1 bar of D_2 is added at −196 °C, and the tube it is left to reach room temperature.

Computational Details. *Energy Profile Calculations.* All calculations were carried out at the DFT level, using the M06 functional[30,37] with an ultrafine grid[38] as implemented in Gaussian09.[39] The geometries of reactants, intermediates, transition states, and products were optimized using basis set I (BS-I). With BS-I, the C, N, and H atoms were described with the 6-31G(d,p) basis set,[40] whereas Pt was described using an effective core potential SDD for the inner electron and its associated double-ζ basis set for the outer ones,[41] complemented with a set of f-polarization functions.[42] Harmonic frequencies were computed analytically with BS-I to classify the stationary points as either minima or saddle points. These calculations were also used to determine the difference between the Gibbs and potential energies in gas phase ($G_{gp} - E_{gp}$), which includes the zero-point, thermal, and entropy corrections. The nature of the transition states was further confirmed by means of IRC calculations[43] with BS-I. The effect of the dichloromethane solvent (ε = 8.93) was estimated by computing the energy in solvent (E_{DCM}) by means of single-point calculations on gas-phase optimized geometries with the solvation model density (SMD) continuum solvation model,[44] using an extended basis set (BS-II). With BS-II, C, N, and H atoms were described with the triple-ζ 6-311++G(d,p) basis set.[45] All the energies given in the text are Gibbs energies in solution, G_{DCM}, which were calculated by adding thermal and entropic corrections to the SMD energies (eq 1).

$$G_{DCM} = E_{DCM}(BS - II) + (G_{gp} - E_{gp})(BS - I) \quad \text{(eq 1)}$$

Molecular Dynamics Simulations. About 1000 dichloromethane molecules were used to solvate the complex in a cubic box of 47.03 Å edges. The simulation cell was treated under periodic boundary conditions. The counteranion [SbF_6]$^-$ was included in the model to neutralize the simulation cell. The organometallic complex was treated quantum mechanically (in a cubic box of 20 Å edge), whereas the solvent molecules and the counteranion were described using molecular mechanics. Dichloromethane (DCM) was described by the fully flexible all-atom potential developed by Kollman and coworkers.[46] The force field was shown to reproduce the macroscopic properties of liquid DCM, including density, heat of vaporization, and diffusion constant, in good agreement with experimental data. Suitable parameters were particularly calculated for the counteranion, using the method developed by Seminario.[47]

Simulations were performed according to the Born−Oppenheimer approach using the CP2K program package.[48,49] The QM subsystem was treated at the DFT level by means of the Perdew−Burke−Ernzerhof (PBE) exchange-correlation functional[24,50] supplemented by the dispersion correction of Grimme et al.[51] Simulations were performed at constant volume and temperature (300 K) through a velocity rescaling thermostat, which guarantees canonical sampling,[52] using a time step of 0.5 fs. The Quickstep algorithm[53] was used to solve the electronic structure problem using a double-ζ plus polarization (DZVP) basis set[54] to represent the orbitals and plane waves (up to 300 Ry) for the electron density. Core electrons were described using pseudopotentials.[55] Wave function optimization was achieved through the orbital transformation method using electronic gradients of 5×10^{-7} as convergence criterion.[56] The QM/MM coupling follows the implementation developed by Laino et al.[57] Initially, the model underwent 0.5 ns classical MD simulation keeping the organometallic complex fixed, and the final conformation was used to start the QM/MM MD simulation.

Buried Volume Calculations. Percentage of buried volume values[34,35] were computed by means of the freely available web application Samb*V*ca.[34b] Default values for the distance from the center of the sphere (2.1 Å) and mesh spacing (0.05) were used. The sphere radius *R* was set at different values ranging from 2.5 to 4.0 Å. Hydrogen atoms were included in all calculations.

X-ray Crystallography. A yellow parallelepiped-shaped crystal of dimensions 0.16 × 0.08 × 0.06 mm^3 was selected under a polarizing optical microscope and was glued on a glass fiber. Data were collected on a Bruker four-circle κ diffractometer equipped with a Cu microsource operated at 30 W power (45 kV, 0.60 mA) to generate Cu Kα radiation (λ = 1.54178 Å) and on a Bruker AXIOM area detector (microgap technology), at room temperature (296 K); exploring over a hemisphere of the reciprocal space in a combination of ϕ and ω scans to reach a resolution of 0.8 Å (62.12° in θ), using the Bruker APEX2 software suite (each exposure of 10 s covered 0.5° in ω). Unit cell dimensions were determined by a least-squares fit of reflections with $I > 2\sigma(I)$. Data were integrated and scaled using *SAINTplus* program.[58] A semiempirical absorption and scale correction based on equivalent reflection was carried out using *SADABS*.[59] Space group determination was carried out using *XPREP*.[60] The structure was solved by direct methods using *SHELXS*,[60] showing all no-hydrogen atoms. The SbF_6 showed its usual positional disorder. Additional cycles of refinement and electron difference maps showed the rest of the hydrogen atoms. Refinement was carried out by anisotropic full-matrix least-squares, except for hydrogen atoms, which were included with isotropic thermal parameter using *SHELXL*;[60] the final cycles had a Pt−H distance antibumping restrained to be great than 1.62(2) Å. The final structure was examined and tested using *PLATON*.[61]

■ ASSOCIATED CONTENT

Ⓢ Supporting Information

Experimental NMR spectra of new complexes at different temperatures; crystallographic information. Cartesian coordi-

dx.doi.org/10.1021/ic500705t | *Inorg. Chem.* 2014, 53, 4257−4268

nates and absolute energies and Gibbs energies (hartrees) in gas phase and in dichloromethane of all the optimized species. QM/MM MD simulation of complex **2c**. This material is available free of charge via the Internet at http://pubs.acs.org.

AUTHOR INFORMATION

Corresponding Authors

*E-mail: agusti@klingon.uab.es. (A.L.)
*E-mail: sconejero@iiq.csic.es. (S.C.)

Notes

The authors declare no competing financial interest.

ACKNOWLEDGMENTS

Financial support from the Spanish Ministerio de Economía y Competitividad (Projects CTQ2010-17476, CTQ2011-23336, and ORFEO CONSOLIDER-INGENIO 2010, CSD2007-00006, and CSD2006-00015, MAT2010-17571) and Junta de Andalucía (Project FQM 2126). FEDER support is acknowledged. O.R.-W., M.A.O., and M.R.-M. thank the Spanish MECD and the CSIC for research grants. The Barcelona Supercomputing Center, Red Española de Supercomputación (BSC-RES) is acknowledged by generous allocation of computer time. We thank Dr. Joaquín López Serrano for assistance with T_1 NMR measurements.

REFERENCES

(1) (a) Dalebrook, A. F.; Gan, W.; Grasemann, M.; Moret, S.; Laurenczy, G. *Chem. Commun.* **2013**, *42*, 8735−8751. (b) Less, R. J.; Melen, R. L.; Wright, D. S. *RSC Adv.* **2012**, *2*, 2191−2199. (c) Weidenthaler, C.; Felderhoff, M. *Energy Environ. Sci.* **2011**, *4*, 2495−2502. (d) Staubitz, A.; Robertson, A. P. M.; Manners, I. *Chem. Rev.* **2010**, *110*, 4079−4124. (e) Smythe, J. C.; Gordon, J. C. *Eur. J. Inorg. Chem.* **2010**, 509−521. (f) Marder, T. B. *Angew. Chem., Int. Ed.* **2007**, *46*, 8116−8118. (g) Stephens, S. H.; Pons, V.; Baker, R. T. *Dalton Trans.* **2007**, 2613−2626.

(2) (a) St. John, A.; Goldberg, K. I.; Heinekey, D. M. *Top. Organomet. Chem.* **2013**, *40*, 271−288. (b) Waterman, R. *Chem. Soc. Rev.* **2013**, *42*, 5629−5641. (c) Alcaraz, G.; Sabo-Etienne, S. *Angew. Chem., Int. Ed.* **2010**, *49*, 7170−7179.

(3) Roselló-Merino, M.; López-Serrano, J.; Conejero, S. *J. Am. Chem. Soc.* **2013**, *135*, 10910−10913.

(4) (a) Campos, J.; Peloso, R.; Carmona, E. *Angew. Chem., Int. Ed.* **2012**, *51*, 8255−8258. (b) Baratta, W.; Stoccoro, S.; Doppiu, A.; Herdtweck, E.; Zucca, A.; Rigo, P. *Angew. Chem., Int. Ed.* **2003**, *42*, 105−108.

(5) For related Pt−C hydrogenations, see Ingleson, M. J.; Mahon, M. F.; Weller, A. S. *Chem. Commun.* **2004**, 2398−2399.

(6) (a) Berke, H. *ChemPhysChem* **2010**, *11*, 1837−1849. (b) Kubas, G. J. *Chem. Rev.* **2007**, *107*, 4152−4205. (c) Heinekey, D. M.; Lledós, A.; Lluch, J. M. *Chem. Soc. Rev.* **2004**, *33*, 175−182.

(7) Ortuño, M. A.; Conejero, S.; Lledós, A. *Beilstein J. Org. Chem.* **2013**, *9*, 1352−1382.

(8) (a) Kubas, G. J. *J. Organomet. Chem.* **2014**, *751*, 33−49. (b) Gordon, J. C.; Kubas, G. J. *Organometallics* **2010**, *29*, 4682−4701. (c) Kubas, G. J. *J. Organomet. Chem.* **2009**, *694*, 2648−2653. (d) Szymczak, N. K.; Tyler, D. R. *Coord. Chem. Rev.* **2008**, *252*, 212−230. (e) Kubas, G. J. *Proc. Natl. Acad. Sci. U.S.A.* **2007**, *104*, 6901−6907.

(9) (a) Tsay, C.; Mankad, N. P.; Peters, J. C. *J. Am. Chem. Soc.* **2010**, *132*, 13975−13977. (b) Kimmich, B. F. M.; Bullock, R. M. *Organometallics* **2002**, *21*, 1504−1507. (c) Stahl, S. S.; Labinger, J. A.; Bercaw, J. E. *Inorg. Chem.* **1998**, *37*, 2422−2431. (d) Butts, M. D.; Scott, B. L.; Kubas, G. J. *J. Am. Chem. Soc.* **1996**, *118*, 11831−11843. (e) Gusev, D. G.; Notheis, J. U.; Rambo, J. R.; Hauger, B. E.; Eisenstein, O.; Caulton, K. G. *J. Am. Chem. Soc.* **1994**, *116*, 7409−7910.

(10) Mas-Ballesté, R.; Lledós, A. H−H Bond Activation. In *Comprehensive Inorganic Chemistry II;* Reedijk, J., Poeppelmeir, K., Eds.; Elsevier: Oxford, 2013; Vol. 9, pp 727−766.

(11) Giunta, D.; Hölscher, M.; Lehmann, C. W.; Mynott, R.; Wirtz, C.; Leitner, W. *Adv. Synth. Catal.* **2003**, *345*, 1139−1145.

(12) Burling, S.; Häller, L. J. L.; Mas-Marzá, E.; Moreno, A.; Macgregor, S. A.; Mahon, M. F.; Pregosin, P. S.; Whittlesey, M. K. *Chem.—Eur. J.* **2009**, *15*, 10912−10923.

(13) (a) Rivada-Wheelaghan, O.; Ortuño, M. A.; Díez, J.; E; Lledós, A.; Conejero, S. *Angew. Chem., Int. Ed.* **2012**, *51*, 3936−3939. (b) Rivada-Wheelaghan, O.; Donnadieu, B.; Maya, C.; Conejero, S. *Chem.—Eur. J.* **2010**, *16*, 10323−10326.

(14) For a related Ir(III) species, see Scott, N. M.; Pons, V.; Stevens, E. D.; Heinekey, D. M.; Nolan, S. P. *Angew. Chem., Int. Ed.* **2005**, *44*, 2512−2515.

(15) Goel, R. G.; Srivastava, R. C. *Can. J. Chem.* **1983**, *61*, 1352−1359.

(16) (a) Nelson, D. J.; Nolan, S. P. *Chem. Soc. Rev.* **2013**, *42*, 6723−6753. (b) Jahnke, M. C.; Hahn, F. E. *Top. Organomet. Chem.* **2010**, *30*, 95−129. (c) Dröge, T.; Glorius, F. *Angew. Chem., Int. Ed.* **2010**, *49*, 6940−6952. (d) Urban, S.; Tursky, M.; Frölich, R.; Glorius, F. *Dalton Trans.* **2009**, 6934−6940. (e) Díez-González, S.; Nolan, S. P. *Coord. Chem. Rev.* **2007**, *251*, 874−883. (f) Scott, N. M.; Nolan, S. P. *Eur. J. Inorg. Chem.* **2005**, 1815−1828. (g) Cavallo, L.; Correa, A.; Costabile, C.; Jacobsen, H. *J. Organomet. Chem.* **2005**, *690*, 5407−5413.

(17) We have used indistinctly complex $[Pt(IPr')(IPr)][BAr^F]$, **1b**, and its counterpart $[Pt(IPr')(IPr)][SbF_6]$, **1b**·SbF_6. Their behavior towards H_2 is identical, but the quality of the crystals of the reaction products from the latter are better.

(18) Brookhart, M.; Green, M. L. H; Parkib, G. *Proc. Natl. Acad. Sci. U.S.A.* **2007**, *104*, 6908−6914.

(19) Ortuño, M. A.; Vidossich, P.; Ujaque, G.; Conejero, S.; Lledós, A. *Dalton Trans.* **2013**, *42*, 12165−12172.

(20) (a) Sajith, P. K.; Suresh, C. H. *J. Organomet. Chem.* **2011**, *696*, 2086−2092. (b) Zhu, J.; Lin, Z.; Marder, T. B. *Inorg. Chem.* **2005**, *44*, 9384−9390.

(21) (a) Braunschweig, H.; Brenner, P.; Dewhurst, R.; Jimenez-Halla, J. O. C.; Kupfer, T.; Rais, D.; Uttinger, K. *Angew. Chem., Int. Ed.* **2013**, *52*, 2981−2984. (b) Arnol, N.; Braunschweig, H.; Brenner, P.; Jimenez-Halla, J. O. C.; Kupfer, T.; Radacki, K. *Organometallics* **2012**, *31*, 1897−1907. (c) Braunschweig, H.; Radacki, K.; Uttinger, K. *Chem.—Eur. J.* **2008**, *14*, 7858−7866. (d) Braunschweig, H.; Radacki, K.; Rais, D.; Scheschkewitz, D. *Angew. Chem., Int. Ed.* **2005**, *44*, 5651−5654.

(22) There is only one report on the X-ray crystallographyc characterization of a three-coordinated Co(I) complex: Ding, K.; Brennessel, W. W.; Holland, P. L. *J. Am. Chem. Soc.* **2009**, *131*, 10804−10805.

(23) (a) Stahl, S. S.; Labinger, J. A.; Bercaw, J. E. *Inorg. Chem.* **1998**, *37*, 2422−2431. (b) Kimmich, B. F. M.; Bullock, R. M. *Organometallics* **2002**, *21*, 1504−1507.

(24) The functional used in the study, PBE, can correctly reproduce agostic bonding situations. (a) Pantazis, D. A.; McGrady, J. E.; Maseras, F.; Etienne, M. *J. Chem. Theory Comput.* **2007**, *3*, 1329−1336. (b) Tognetti, V.; Joubert, L.; Cortona, P.; Adamo, C. *J. Phys. Chem. A* **2009**, *113*, 12322−12327.

(25) A closely related example has been reported: Languérand, A.; Barnes, S. S.; Bélanger-Chabot, G.; Maron, L.; Berrouard, P.; Audet, P.; Fontaine, F.-G. *Angew. Chem., Int. Ed.* **2009**, *48*, 6695−6698.

(26) Hydrogenation of derivatives **1a**−**c** does also take place in THF, but coordination of this solvent to the final hydrogenated $[PtH(NHC)_2]^+$ products is not observed after removal of volatiles and redissolution in dichloromethane.

(27) Siedle, A. R.; Newmark, R. D.; Gleason, W. B. *J. Am. Chem. Soc.* **1986**, *108*, 767−780.

(28) Connelly, S. J.; Zimmerman, A. C.; Kaminsky, W.; Heinekey, D. M. *Chem.—Eur. J.* **2012**, *18*, 15932−15934.

(29) (a) Devarajan, D.; Ess, D. H. *Inorg. Chem.* **2012**, *51*, 6367−6375. (b) Vastine, B. A.; Hall, M. B. *J. Am. Chem. Soc.* **2007**, *129*, 12068−

12069. (c) Perutz, R. N.; Sabo-Etienne, S. *Angew. Chem., Int. Ed.* **2007**, *46*, 2578−2592.
(30) (a) Zhao, Y.; Truhlar, D. G. *Acc. Chem. Res.* **2008**, *41*, 157−167. (b) Zhao, Y.; Truhlar, D. G. *Chem. Phys. Lett.* **2011**, *502*, 1−13.
(31) The Gibbs activation energy in solvent could be overestimated by the use of gas-phase entropic corrections.
(32) (a) Paton, R. S.; Seonah Kim, S.; Ross, A. G.; Danishefsky, S. J.; Houk, K. N. *Angew. Chem., Int. Ed.* **2011**, *50*, 10366−10368. and references therein. (b) van Zeist, W.-J.; Bickelhaupt, F. M. *Org. Biomol. Chem.* **2010**, *8*, 3118−3127.
(33) Since all complexes **3** contain a hydride ligand in trans position to H_2, the interaction energy is assumed to be rather similar. Entropic factors are also assumed to apply in a similar extent.
(34) (a) Hillier, A. C.; Sommer, W. J.; Yong, B. S.; Petersen, J. L.; Cavallo, L.; Nolan, S. P. *Organometallics* **2003**, *22*, 4322−4326. (b) Poater, A.; Consenza, B.; Correa, A.; Giudice, S.; Ragone, F.; Scarano, V.; Cavallo, L. *Eur. J. Inorg. Chem.* **2009**, 1759−1766.
(35) Clavier, H.; Nolan, S. P. *Chem. Commun.* **2010**, *46*, 841−861.
(36) Maseras, F.; Lledós, A.; Clot, E.; Eisenstein, O. *Chem. Rev.* **2000**, *100*, 601−636.
(37) Zhao, Y.; Truhlar, D. *Theor. Chem. Acc.* **2008**, *120*, 215−241.
(38) Wheeler, S. E.; Houk, K. N. *J. Chem. Theory Comput.* **2010**, *6*, 395−404.
(39) Frisch, M. J. et al. *Gaussian 09,* Revision A.1; Gaussian, Inc.: Wallingford, CT, 2009.
(40) (a) Hehre, W. J.; Ditchfield, R.; Pople, J. A. *J. Chem. Phys.* **1972**, *56*, 2257−2261. (b) Francl, M. M.; Pietro, W. J.; Hehre, W. J.; Binkley, J. S.; Gordon, M. S.; DeFrees, D. J.; Pople, J. A. *J. Chem. Phys.* **1982**, *77*, 3654−3665.
(41) Andrae, D.; Häußermann, U.; Dolg, M.; Stoll, H.; Preuß, H. *Theor. Chim. Acta* **1990**, *77*, 123−141.
(42) Ehlers, A. W.; Böhme, M.; Dapprich, S.; Gobbi, A.; Höllwarth, A.; Jonas, V.; Köhler, K. F.; Stegmann, R.; Veldkamp, A.; Frenking, G. *Chem. Phys. Lett.* **1993**, *208*, 111−114.
(43) (a) Hratchian, H. P.; Schlegel, H. B. *J. Chem. Phys.* **2004**, *120*, 9918−9924. (b) Hratchian, H. P.; Schlegel, H. B. *J. Chem. Theory Comput.* **2005**, *1*, 61−69.
(44) Marenich, A. V.; Cramer, C. J.; Truhlar, D. G. *J. Phys. Chem. B* **2009**, *113*, 6378−6396.
(45) (a) Clark, T.; Chandrasekhar, J.; Spitznagel, G. W.; Schleyer, P. V. R. *J. Comput. Chem.* **1983**, *4*, 294−301. (b) Krishnan, R.; Binkley, J. S.; Seeger, R.; Pople, J. A. *J. Chem. Phys.* **1980**, *72*, 650−654.
(46) Fox, T.; Kollman, P. *J. Phys. Chem. B* **1998**, *102*, 8070−8079.
(47) Seminario, J. M. *Int. J. Quantum Chem.* **1996**, *60*, 1271−1277.
(48) Hutter, J.; Iannuzzi, M.; Schiffmann, F.; VandeVondele, J. *WIREs Comput. Mol. Sci.* **2014**, *4*, 15−25.
(49) VandeVondele, J.; Krack, M.; Mohamed, F.; Parrinello, M.; Chassaing, T.; Hutter, J. *Comput. Phys. Commun.* **2005**, *167*, 103−128.
(50) Perdew, J. P.; Burke, K.; Ernzerhof, M. *Phys. Rev. Lett.* **1996**, *77*, 3865−3868.
(51) Grimme, S.; Antony, J.; Ehrlich, S.; Krieg, H. *J. Chem. Phys.* **2010**, *132*, 154104.
(52) Bussi, G.; Donadio, D.; Parrinello, M. *J. Chem. Phys.* **2007**, *126*, 014101.
(53) Lippert, G.; Hutter, J.; Parrinello, M. *Mol. Phys.* **1997**, *92*, 477−487.
(54) VandeVondele, J.; Hutter, J. *J. Chem. Phys.* **2007**, *127*, 114105.
(55) (a) Goedecker, S.; Teter, M.; Hutter, J. *Phys. Rev. B* **1996**, *54*, 1703−1710. (b) Krack, M. *Theor. Chem. Acc.* **2005**, *114*, 145−152.
(56) VandeVondele, J.; Hutter, J. *J. Chem. Phys.* **2003**, *118*, 4365−4369.
(57) Laino, T.; Mohamed, F.; Laio, A.; Parrinello, M. *J. Chem. Theory Comput.* **2005**, *1*, 1176−1184.
(58) *SAINTplus* package; Bruker AXS, Inc.: Madison, WI, 2006.
(59) Sheldrick, G. M. *SADABS* program integrated in *APEX2* package; Bruker AXS, Inc.: Madison, WI, 2009.
(60) Sheldrick, G. M. *XPREP, SHELXS, and SHELXL* programs integrated in *APEX2* package; Bruker AXS, Inc.: Madison, WI, 2008.
(61) Spek, A. L. *PLATON, A multipurpose Crystallographic Tool*; Utrecht University: Utrecht, Holland, 2005.